Nanoplasmonics for Dual-Molecule Release through Nanopores in the Membrane of Red Blood Cells

Mihaela Delcea,[†,§,△,*] Nadine Sternberg,[‡,△] Alexey M. Yashchenok,[†] Radostina Georgieva,[‡,⊥] Hans Bäumler,[‡] Helmuth Möhwald,[†] and Andre G. Skirtach[†,∥,#,*]

[†]Department of Interfaces, Max-Planck Institute of Colloids and Interfaces, Research Campus Golm, Golm 14424, Germany, [§]ZIK HIKE, Ernst-Moritz-Arndt-Universität Greifswald, Greifswald 17489, Germany, [‡]Center of Tumor Medicine, Berlin Brandenburg Center for Regenerative Therapies, Charité-Universitätsmedizin-Berlin, Berlin 10117, Germany, [⊥]Department of Medical Physics, Biophysics and Radiology, Medical Faculty, Trakia University, ul. Armeiska 11, 6000 Stara Zagora, Bulgaria, [∥]Department of Molecular Biotechnology, Ghent University, Ghent 9000, Belgium, and [#]NB-Photonics, Ghent University, Ghent 9000, Belgium. [△]These authors contributed equally to this work.

ABSTRACT

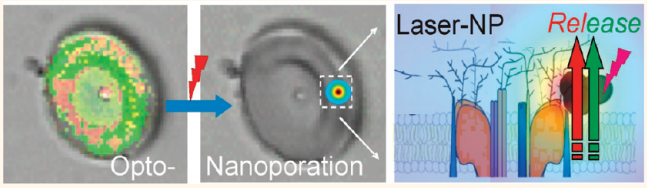

A nanoplasmonics-based opto-nanoporation method of creating nanopores upon laser illumination is applied for inducing diffusion and triggered release of small and large molecules from red blood cells (RBCs). The method is implemented using absorbing gold nanoparticle (Au-NP) aggregates on the membrane of loaded RBCs, which, upon near-IR laser light absorption, induce release of encapsulated molecules from selected cells. The binding of Au-NPs to RBCs is characterized by Raman spectroscopy. The process of release is driven by heating localized at nanoparticles, which impacts the permeability of the membrane by affecting the lipid bilayer and/or trans-membrane proteins. Localized heating and temperature rise around Au-NP aggregates is simulated and discussed. Research reported in this work is relevant for generating nanopores for biomolecule trafficking through polymeric and lipid membranes as well as cell membranes, while dual- and multi-molecule release is relevant for theragnostics and a wide range of therapies.

KEYWORDS: nanoplasmonics · trans-membrane · channel proteins · lipid bilayers · gold nanoparticles · localized heating · RBC · nanopores

The cellular membrane is highly selective, as it represents an effective barrier for most charged, noncharged, and polar molecules.[1] However, one can take advantage of this impermeability to design a natural drug carrier. The development of biologically inspired drug delivery systems is advantageous in comparison with conventional administration of therapeutics. This allows for reduction of both toxicity and adverse side effects while keeping the drug concentration in the blood within the therapeutic window, protection from premature inactivation, and loss of its systemic activity.[2] Red blood cells (RBCs) represent an interesting drug carrier system due to their inherent biocompatibility and long systemic circulation. Their membranes can be reversibly opened and closed (resealed), allowing encapsulation of a broad spectrum of drugs, enzymes, and any other biologically active substances (see ref 3 for a review). In 1985, Alpar and colleagues published the *in vivo* therapy of implanted TLX5 tumor cells with methotrexate-loaded carrier-RBCs as anticancer treatment.[4] Recently, our group showed the selective administration of amphotericin B-loaded RBCs to macrophages of the reticuloendothelial system.[5] Encapsulation of superparamagnetic iron oxide nanoparticles[6] and thermosensitive magnetite nanoparticles[7] into RBCs was introduced as a novel strategy for magnetic resonance imaging. RBCs can be also manipulated[8] for positioning and lab-on-chip applications[9−11] or can be used as carriers of nanoparticles.[12,13] However, triggering the cargo release from RBCs at a desired site with a defined time sequence and quantities has not been extensively studied to-date.

Previously, photodynamic hemolysis was studied using CW (continuous wave) sources for RBCs in the presence of dyes[14] that have high extinction coefficients and peak absorption in the UV−visible region, for example Rose Bengal[15] or phenol red.[16,17] In addition to CW irradiation, pulsed sources[18] can be used (see ref 19 for a review). In this case extremely high laser peak powers (~10^{12} W/cm^2),[20] which can damage RBCs, are used.[21] Comparison of heat generation by pulsed and CW lasers has been presented earlier.[22]

Among numerous stimuli[23] and release methods[24] we have chosen laser−nanoparticle interaction, *i.e.*, nanoplasmonics,[25] to study

* Address correspondence to mihaela.delcea@mpikg.mpg.de; skirtach@mpikg.mpg.de.

Received for review February 14, 2012 and accepted March 31, 2012.

Published online April 01, 2012
10.1021/nn3006619

release from RBCs. Noble metal nanoparticles were used previously to target cancer cells,[26,27] to investigate phase transitions[28,29] and transfer of nanoparticles through the lipid membrane,[30] and to induce release from capsules[31−34] and liposomes (see refs 35, 36 for review). These effects are based on localized heat generated by laser−nanoparticle interaction. The permeability changes of these delivery vehicles can be termed laser-assisted opto-nanoporation because of the highly localized effects on the membrane. Nanoparticles can also extend the scope of permeability control of RBCs. They would enable, for example, application of low-power laser sources, which do not affect the membrane of the cells[37] due to minimal absorption of near-infrared light[38] by the membrane molecules and water.[39] This technique is noninvasive and is ideally suited to investigate cells, polymeric capsules inside living cells,[37,40,41] and films.[42−44]

The goals of this work are twofold. On one hand, providing the means for nanoscale manipulation of the RBC membrane permeability should open new perspectives for designing carriers. The very new challenge here consists in triggering the drug release at a desired site with defined time sequence and quantities. On the other hand, opto-nanoporation has the potential to find application as a new tool for studying stimuli-responsive cross-membrane transport of molecules. We study here the permeability changes of the nanoparticle-functionalized membrane of RBCs upon laser irradiation and report on the laser-assisted controlled release of model drugs encapsulated in the RBC interior. Simultaneous release of two molecules, the dye 5(6)-carboxyfluorescein (5(6)-CF) and a rhodamine-labeled dextran (Rh-dextran), with different molecular masses of 376 and 7500 Da, respectively, is conducted. Practically, our approach is relevant for delivery of a combination of drugs, which is often needed, for example, in the treatment of cancer.[45−47]

RESULTS AND DISCUSSION

Experiments were carried out according to the scheme presented in Figure 1. In the first step, the biopolymer Rh-dextran and the dye 5(6)-CF were simultaneously loaded into RBCs, Figure 1 (step 1). Here we used a hypotonic dilution−encapsulation method[48] of these two molecules into RBCs. The procedure is based on the process of hypotonic hemolysis, during which, upon influx of water, pores with a diameter of up to 100 nm occur in the membrane and hemoglobin diffuses out of the cells. At low temperature, the lifetime of these pores is long enough to allow concentration equilibration between the inner volume of the cells and the dispersion medium. In such a way, materials from the surrounding medium can pass through the membrane. After reconstitution of isotonicity, the cell membrane can be resealed by restoration of osmolarity and increasing the temperature to 37 °C, thus trapping all substances that diffused into the interior of the cell, Figure 1 (step 1). During hypo-osmotic loading, a part of the hemoglobin (roughly 50%) is exchanged against the loaded substances (model drugs, buffers) and the cell volume slightly decreases. The consequence of these changes is an increased stability of the loaded erythrocytes against hypo-osmotic conditions.[49] The optimized protocol applied in this study allows efficient loading with minimized damage of the cell membrane, as shown by Annexin V binding assays[50] (less than 10% Annexin V binding cells). In addition, Supporting Information as well as images in this article show loaded RBCs with high intracellular fluorescence intensity in both fluorescein (green) and rhodamine (red) channels as well as a preserved biconcave shape of the cells.

The second step in our work involves functionalization of RBCs with noble metal nanoparticles as laser light absorption centers, Figure 1 (step 2). These absorption centers are needed because a low-power CW near-IR laser (power and power densities in the range of mW and kW/cm^2 to MW/cm^2, respectively) does not influence the permeability of the membrane and consequently will not induce a release.[37] In this step, highly concentrated gold nanoparticles (Au-NPs) were added to the RBC suspension in PBS (phosphate-buffered saline, 0.15 M NaCl, 0.01 M phosphate buffer, pH 7.4). Such a mixing-initiated aggregation of gold nanoparticles takes place simultaneously with adsorption onto the surface of RBCs. It has been shown that the presence of small aggregates increases the efficiency of opto-nanoporation of capsules.[51] Besides the size (5−10 nm) and shape (spherical), one needs to control the spatial distribution of nanoparticles on the membrane surface with regard to their aggregation state. Here, the approaches differ depending on the relative concentration (high[52] or low[53]) of nanoparticles, which themselves tend to form aggregates upon adsorption at high concentration[52] or screening (for example, by salt) of stabilizing repulsive forces.[51] To minimize effects on the membrane fluidity of RBCs, we used a combination of both approaches by adding a small amount of highly concentrated gold nanoparticles (∼1/100 volume dilution) to a RBC suspension in PBS. These nanoparticles are very stable in water, having a ruby-red color, but they aggregate in PBS, turning rapidly (within 1 min) to a blue-gray color (Figure 1 (step 2)). Figure S1 presents absorbance spectra of gold nanoparticles in water (red curve) and in PBS (blue curve). It can be seen that a surface plasmon resonance peak of gold nanoparticles in water is located at 520 nm. After aggregation of gold nanoparticles in PBS, the peak is shifted by ∼50 nm in the near-infrared part of the spectrum. Curves presented in Figure S1 are normalized, and, therefore, absorbance at ∼830 nm is not as high compared to that at ∼520 nm. Similar characteristics were observed by other groups.[54] However, the localized temperature rise is proportional to

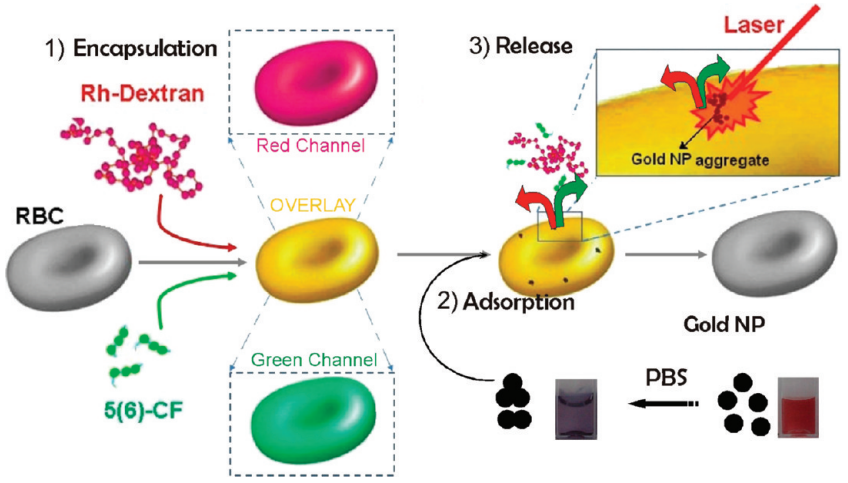

Figure 1. Schematic of the experiments showing three steps: (1) encapsulation: two molecules (Rh-dextran (in red) and 5(6)-CF (in green)) are simultaneously encapsulated. Red, green, and overlay fluorescence channels are shown in the schematics; (2) adsorption of nanoparticle aggregates onto the surface of loaded RBCs (cuvettes demonstrating the behavior of gold nanoparticles in water (right) and after transfer in PBS (left); and (3) release of both molecules by a near-IR laser.

the cube of the size of the nanoparticles.[34,55] Release of encapsulated materials from microcapsules by opto-nanoporation was observed using silver[31] and gold[51] nanoparticle aggregates. Consequently, the still localized heat generated by the Au-NP aggregates should be sufficient to affect also the membrane permeability of the RBCs.

Adsorption of Au-NPs onto RBC membranes (step 2 in Figure 1) is further discussed now. TEM (transmission electron microscope) micrographs used for identification of nanoparticles adsorbed onto RBCs are shown in Figure 2a. It can be seen that single Au-NPs are distributed over the surface of the cells and that some aggregates are also present, Figure 2b. Au-NPs are known for their properties as surface-enhanced Raman scattering (SERS) centers,[56,57] which we use in this study to probe their binding to the membrane of RBCs.[58] Figure 2c demonstrates Raman spectra of Au-NP aggregates along with the SERS-amplified signal. Some of the groups typical for lipids and/or proteins as well as some characteristic of the glycocalix can be distinguished from these spectra (the two solid lines in Figure 2c represent spectra taken at different sites on RBCs possessing Au-NP aggregates). Some peaks in the region 1000−1200 cm^{-1} can be assigned to saccharides. In both spectra presented in Figure 2c peaks at 1083, 1109, and 1174 cm^{-1} were observed;[59] the latter is specific for saccharides only. The broad Raman peak around 1300 cm^{-1} can be assigned to the CH_2 twist of the long alkyl chain in the phospholipids.[60] The peak at 1450 cm^{-1} is assigned to CH_2 (aliphatic chain) and CH_3 bends in lipid bands, respectively. The phospholipid bands include also the O−P−O vibrations of the polar head at 1083 cm^{-1} and C−C stretches[61] of chain at 1109 cm^{-1}. Several peaks in the presented spectra can be assigned to proteins: the peak at 1109 cm^{-1} can be also assigned to C−C and C−N stretching, while the band around 1450 cm^{-1} is assigned to a CH_2 bond. The band around 873 cm^{-1} on the Raman spectrum was detected in both RBC spectra (the peak appears stronger in the upper graph); this band was reported as a typical signal for other sialosides[62] as a result of the COH deformation of their glycerol part.[62]

The scheme of the interactions of Au-NPs with RBCs is presented in Figure 2d. The main interactions of Au-NP aggregates and RBCs depicted in this figure reflect data obtained by Raman scattering data, Figure 2c. The preferable adsorption and aggregation of the gold nanoparticles on the RBC surface is most likely due to interactions of the positively charged nanoparticles with the negative charges of the glycocalyx, as depicted in Figure 2d. The glycocalyx is a coat of fuzzy material, consisting of carbohydrate-rich molecules, polysaccharides, proteoglycans, glycoproteins, and glycolipids.[64] The major part of its negative charges is contributed by sialic acids in the oligosaccharide chains of membrane glycoproteins and glycolipids.[65,66] Interactions with the polar heads of the phospholipids are also possible, mainly with phosphatidylcholine and sphingomyelin, which are the major components in the outer lipid layer.[67,68] The negatively charged membrane lipids such as phosphatidylserine and phosphatidylinositol are mainly placed in the inner leaflet and, therefore, cannot contribute to the NP adsorption.[69] Finally, van der Waals and hydrophobic interactions between the nanoparticles and the cell membrane cannot be completely neglected since electrostatic interactions are screened at physiological ionic strengths.

According to this description, at least three mechanisms affecting the membrane by local heat are feasible:

(i) the local temperature rise can drastically enhance the mobility of lipid molecules and can cause a local phase transition in the lipid bilayer, finally leading to the opening of short-living hydrophilic pores;

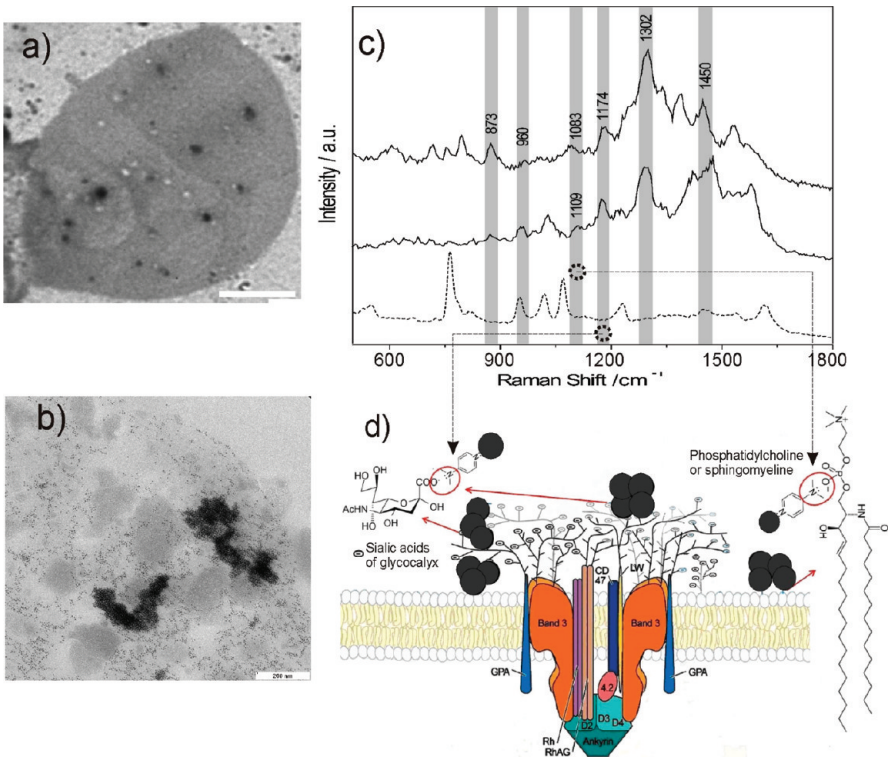

Figure 2. (a) Transmission electron micrograph (TEM) of whole RBCs with adsorbed gold nanoparticle aggregates (the scale bar corresponds to 2 μm); (b) a magnified TEM image of the RBC membrane showing nanoparticles and nanoparticle aggregates (the scale bar corresponds to 200 nm); (c) surface-enhanced Raman spectra (SERS) of vibrational groups of lipids and glycocalix amplified by Au-NPs; two spectra recorded at different locations on the RBCs are presented by solid lines. The spectrum of Au-NPs themselves is also presented by the dashed line; (d) schematic of possible interactions of Au-NPs with the membrane of RBCs at the molecular level (membrane scheme is modified after Salomao *et al*.[63]). Positively charged Au-NPs (black circles, not to scale) are shown interacting with the negatively charged glycocalyx and with the polar heads of phospholipids. The dashed arrow-lines from circles in (c) are specific only to the interactions shown in (d).

(ii) integral glycoproteins located near gold nanoparticles can undergo thermal denaturation, creating rigid hydrophilic pores;

(iii) reactive oxygen species and free radicals can be formed, which can start a damaging chain reaction of lipid peroxidation followed by decreased hydrophobicity of the lipid bilayer.[70]

In the third and last step shown in Figure 1, selected RBCs with Au-NP aggregates were illuminated by a near-IR laser mounted in a microscope setup (step 3). The RBCs were imaged before and after illumination using a confocal laser scanning microscope (CLSM); in separate experiments they were also imaged during illumination by a near-IR laser using fluorescence imaging. We discuss now this step in more detail.

Experimental examples of release from RBCs are demonstrated in Figures 3–5. Figure 3.1 presents the simultaneous release of the co-encapsulated 5(6)-CF and Rh-dextran from a single RBC upon laser irradiation. In Figure 3.1a three RBCs are shown in an overlay image of transmission and red and green fluorescence channels. The yellow color is due to the combination of the green color of 5(6)-CF (presented in Figure 3.1b) and the red color of the Rh-dextran (depicted in Figure 3.1c). Only one (in the dashed white box) of the three imaged RBCs was illuminated by a near-IR laser. Figure 3.1d shows the same three cells after illumination. It can be clearly seen from this figure that nonilluminated cells retain their fluorescence, while the illuminated one becomes completely dark, suggesting release of the fluorescing molecules, Figure 3.1d. The green and red channels of the illuminated RBC are demonstrated in Figure 3.1e,f. It is evident from Figure 3.1 that all cells, also the illuminated one, maintain a biconcave, disk-like, shape, Figure 3.1d, while both fluorescent channels demonstrate that encapsulated molecules were released only from the illuminated RBC, Figure 3.1e,f. It can be emphasized that the biconcave or disk-like shape of the RBC is unchanged before illumination (Figure 3.1a–c) and after release (Figure 3.1d–f) of the encapsulated materials. RBCs can possess a number of different shapes,[71] while another common shape of RBCs is echinocytes. To additionally prove that release by opto-nanoporation has no influence on the shape of RBCs, we have also conducted release from echinocytes. The echinocytic shape was induced by addition of a small amount of acetylsalicylic acid to the RBC suspension. Figure 3.2 shows images of an echinocyte before (a1–a3) and after (b) laser illumination. Different planes of

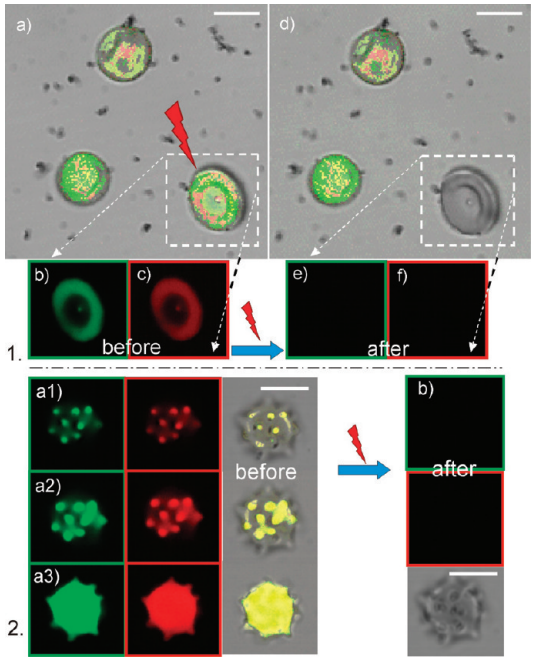

Figure 3. (1) CLSM images of RBCs with co-encapsulated 5(6)-CF and Rh-dextran molecules before (a−c) and after (d−f) laser-induced opto-nanoporation. Panels (a) and (d) present overlays of green and red fluorescence and transmission channels. Red and green channels of the single RBC in the dashed box are shown separately before (b, c) and after (d−f) release, respectively. Au-NP aggregates were not removed in this case and are seen as dark dots. Scale bars correspond to 5 μm. (2) CLSM images of an echinocyte with co-encapsulated 5(6)-CF and Rh-dextran molecules are shown before (a1−a3) and after (b) laser-induced opto-nanoporation. Gray background panels represent overlays of all fluorescence and transmission channels. (a1), (a2), and (a3) show different confocal image planes of the same echinocyte; (b) shows the middle section, while other sections of this echinocyte are presented in Figure S2. Scale bars correspond to 5 μm.

imaging in Figure 3.2a1−a3 demonstrate uniformity of loading of the echinocyte. It can be clearly seen from Figure 3.2b) that fluorescence is no longer present after laser exposure.

In order to demonstrate the release in more detail, we recorded and analyzed *in situ* the illumination process (Methods). Frame-by-frame analysis of illumination is presented in Figure 4. The laser was turned on only in frames (b)−(e), and its location is marked by the red circle. The cloud shown in Figure 4d,e depicts release of 5(6)-CF molecules during the illumination. It can be noticed from Figure 4e that release is directional; that is, radially asymmetric. An analogous phenomenon has been reported for release from microcapsules.[72,73] Similarly to Figure 3, RBCs that were not illuminated retained their fluorescence even after release from the RBCs pointed out by the blue arrow, Figure 4h,i. The diffusion constants of fluorescein and dextran (for example, 9 kD) in aqueous solution are $\sim 2 \times 10^{-6}$ cm$^2 \cdot$s^{-1} and 5×10^{-7} cm$^2 \cdot$s^{-1}, respectively (and they decrease by a factor of ~4 in the cytoplasm of cells[74]). For ~7 μm RBCs (a typical average size of the disk of RBCs), these molecules would need ~0.1 s to cross the distance corresponding to the diameter of the disk of an RBC. Opto-nanoporation takes place during the time of illumination, which was performed on the order of seconds per cell. During this time period, molecules can cross the whole RBC. It can be noted that no attachment of molecules to structures inside the cell occurs because no intracellular structures exist in RBCs. There is also no chemical or electrostatic interaction of dextran and 5(6)-CF with the actin/spectrin network or with the lipid bilayer. This is also evident from the continuous distribution of fluorescence intensity inside a RBC, *i.e.*, without any enhancement in any region of the membrane.

Although release from RBCs was visualized *in situ*, Figure 4, we conducted additional negative control experiments to exclude (a) photobleaching by the lamp; (b) photobleaching by the near-IR laser, and (c) thermobleaching. To exclude photobleaching by the fluorescence lamp, we have visualized several cells (for example, Figures 3 and 4). Photobleaching by the lamp would equally extinguish signals from all RBCs, while in our experiments only the exposed cell appeared empty after near-IR laser illumination. Photobleaching by laser was excluded by exposing loaded RBCs without nanoparticles to the laser; here, RBCs remained highly fluorescent even after prolonged illumination (Figure S3, Supporting Information). With regard to thermobleaching, we conducted an experiment with stained-membrane RBCs loaded with 5(6)-CF (green fluorescence signal), Figure 5.

In this sample the RBC membranes were stained by a hydrophobic dye, PKH26 (Methods), to provide a "fixed" red fluorescence signal (Figure 5). After laser illumination of the cell, pointed out by the blue arrow, the green signal disappeared, while the red fluorescence could still be visualized in the shell, Figure 5b. Here, 5(6)-CF is entrapped in the interior of the RBCs without binding to cellular structures, and it can escape by diffusion as soon as the membrane barrier is opened. In contrast, PKH26 is incorporated in the membrane lipid layer and cannot be released by opto-nanoporation. Thus, Figure 5 again demonstrates release from RBCs and serves as a negative control for thermobleaching since the red fluorescence in the membrane was not impaired. These effects are expected due to the strongly localized[75] effects of heating.

Noble metal nanoparticles convert electromagnetic waves into heat,[76−84] a feature often used for fabrication at the nanoscale.[85−88] The heat rise upon laser illumination was both measured[34,89] and calculated,[55] including conditions of different surrounding media.[90] This process takes place on the nanometer scale, and, applied to our study here, it can locally perturb the membrane, thus leading to generation of pores and

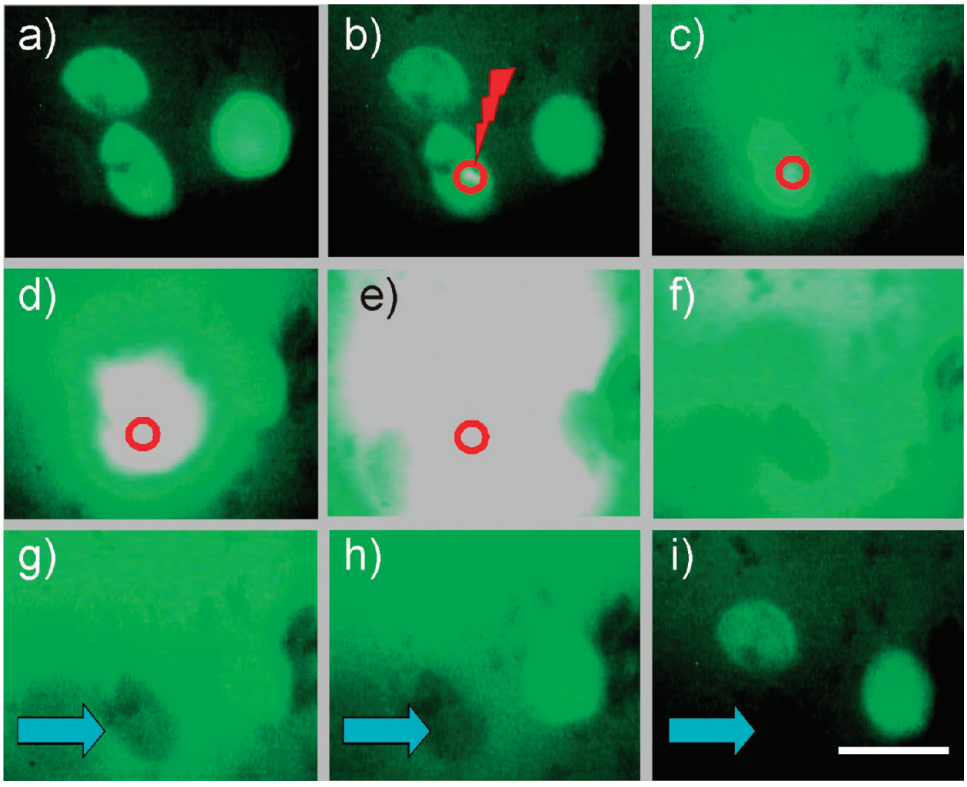

Figure 4. Frame-by-frame *in situ* analysis demonstrating release from a RBC upon laser illumination. The red circle identifies the location of the laser, which is present only in frames (b) through (e). The blue arrows point to the RBC from which the contents were released. The contrast in all frames was decreased for clarity of images; the white areas in images (d) and (e) correspond to oversaturated signal. In the presented sequence (a) was recorded at 0, (b) 23.5, (c) 32.2, (d) ~33.1, (e) ~33.4, (f) 34.5, (g) 35, (h) 36, and (i) 40 s. Positioning of the RBCs under the laser was conducted by the XYZ stage. Image (i) was recorded over 6 s after the laser was switched off. The scale bar pertaining to all images corresponds to 10 μm.

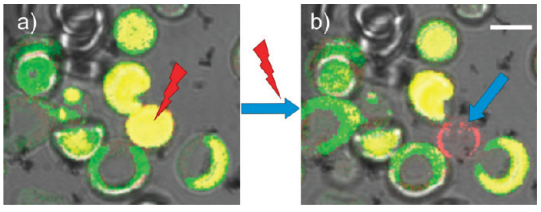

Figure 5. Release from loaded RBCs with labeled membrane: (a) CLSM image of cells; (b) after near-IR laser illumination on the RBCs, indicated by the blue arrow, the green fluorescence signal from this cell disappears, but its shell still exhibits red fluorescence. The scale bar corresponds to 5 μm.

increasing the permeability which should result in release of encapsulated molecules. The size of pores generated in the membrane depends on the size[30] of nanoparticles or their aggregate, as the temperature rise is inversely proportional to the distance[90] from the nanoparticles.

A linear chain of five aggregated nanoparticles upon application of near-IR light can produce up to 10 degrees of localized temperature rise.[51] Larger aggregates will produce a higher temperature increase, but most importantly, the temperature rise is highly localized (to nanoparticles and nanoparticle aggregates). It decays quickly, decreasing to ambient temperature within a distance of several diameters[90] of nanoparticles or nanoparticle aggregates, and it can be controlled by incident laser power or the size of nanoparticles or their aggregates.

We further discuss modeling of the temperature rise,[80,91,92] which is linearly proportional to incident laser power and absorption coefficient.[34] Au-NPs possess a strong surface plasmon resonance peak around 520 nm (or ~2.39 eV). Upon aggregation, longitudinal modes provide the highest shift of the second peak, while the transverse modes stay closer to the surface plasmon resonance peak. In the case of aggregates, a linear chain of nanoparticles and other aggregated states provide a substantial shift noted in the extinction spectrum at higher wavelengths:[93,94] In the case of two nanoparticles only a linear aggregate is possible; longitudinal mode excitation shifts the second peak to ~2.3 eV (for 10 nm nanoparticles).[93,95] In the case of three particles in an aggregate three (in-plane) situations are possible, with the second peak located around 2.1−2.2 eV (for 10 nm nanoparticles).[96] Only a longitudinal mode of the linear chain of nanoparticles (and modes split by the vertex angle[97]) produces a distinct peak located at ~2.22 eV. For transverse modes the excitation peak stays at ~2.4 eV. An aggregate hosts a number of interacting nanoparticles, and although most

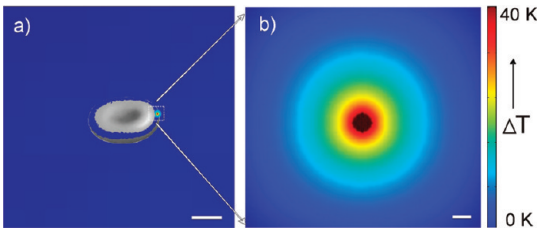

Figure 6. Simulation of the temperature rise, ΔT, and its distribution around (a) a Au-NP aggregate on a RBC and (b) enlarged area around the aggregate in the plane perpendicular to the incident wave. Scale bars correspond to 3 μm and 150 nm in (a) and (b), respectively.

contribution comes from scattering,[98] some contribution to absorption, including its red-shift, occurs.[99]

We modeled temperature rise upon excitation at the surface plasmon resonance peak, where the exact analytical solution of the absorption coefficient and temperature rise exists. Such a calculation provides somewhat of an overestimate of the temperature rise compared to that with the near-IR laser excitation;[93] however, as demonstrated in Figures 3–5 such a temperature rise is sufficient to induce release of substances from RBCs. Thus, release takes places through pores as demonstrated for capsules[100] generated by opto-nanoporation. We present results of modeling of the temperature distribution around a Au-NP aggregate located on a RBC, Figure 6a. The approximate size of aggregates (~150 nm, after 10–20 min of aggregation) was estimated from dynamic light scattering experiments performed in the same PBS buffer, Figure S4. Calculations presented in Figure 6b demonstrate that the temperature rise is highly localized, *i.e.*, around aggregates.

The basic underlying principles driving the release of two distinct molecules from RBCs demonstrated in this work—changing the permeability of the membrane by localized heating and nanoplasmonics[101]—are similar to those reported for microcapsules functionalized with nanoparticles.[102] In the latter case, release was demonstrated inside living cells,[37,40,103] including neurons[104] and cancer cells,[105] and by transiently opening and closing the polymeric membrane.[100] The fact that their shape is unaltered after release (Figures 3–5) serves as an essential indication of the localized effect[28] of opto-nanoporation.

In sharp contrast to the localized temperature effect described above, global heating has a profound effect on RBCs as well as their deformability, ion permeability, and aggregation behavior. RBCs start showing changes of shape and shear modulus at temperatures above 47 °C.[106,107] For example, their shear modulus increases by 30% at 47 °C. Above 46 °C after a lag period, the ion leakage from the RBCs increases, leading to shape changes, vesiculation, and finally thermal hemolysis.[108,109] These effects are strongly dependent on temperature and time of exposure. It is important to underline that in those experiments, the whole suspension containing RBCs was heated. This is very different compared with experiments reported in this work, wherein we have only a local temperature increase, while global (micrometer- and large-scale) temperature rise is insignificant. In the case of capsules global temperature increase allows for encapsulation,[24] while local temperature increase leads to release. Here, the laser has been applied only for a short time period (on the order of seconds), and no prolonged exposure occurred. Also, temperature rise upon near-IR laser–nanoparticles interaction was measured,[34] and nonthermal effects can also influence the permeability.[110]

In other work, nanoparticles have been studied for interaction with DNA[111] as well as with Cos-1 cells and RBCs.[112] Increasing the concentration of nanoparticles led to an increased hemolysis of cells; so in the current work the ratio of nanoparticles to cells was kept low to prevent lysis. In addition to the approach demonstrated in this work, absorbing anisotropic particles (for example, nanorods) can be used. Nanorods[113–116] as well as carbon nanotubes[117] are also quite efficient absorption centers in the near-IR part of the spectrum and have been applied to capsules (refer to ref 24 for a review). It can be noted that our approach can be applied to various delivery carriers.[118,119] In regard to potential *in vivo* applications the proposed approach can be used for remote activation close to the skin, while potential penetration depth limitations may be tackled by combining opto-nanoporation with techniques and devices such as those applied in endoscopic microsurgery, microinjectors, and optical fibers or magnetic fields.[120–122]

CONCLUSIONS

We have introduced nanoplasmonics-based opto-nanoporation of the membrane of RBCs. Release of two distinct molecules by near-IR light has been achieved while preserving the shape of RBCs; this effect has been demonstrated for discocytes as well as for echinocytes. It is shown that gold nanoparticles aggregate in PBS at high concentration and form active laser light absorption centers. Nanoparticle binding to RBCs is monitored by Raman scattering. Results reported in this work (a) provide the basis for study of the permeability of RBCs (as well as other drug delivery vehicles and membranes), (b) identify this nanoplasmonics approach as a useful method in studying the permeability and thermodynamics of permeability of lipid membranes containing oligosaccarides and proteins, and (c) establish multiple-molecule delivery and release from carriers such as RBCs. Temperature rise around nanoparticle aggregates is simulated numerically while taking into account an exact analytical solution. Manipulation of RBCs[8,9]—fully biological and

biocompatible drug carriers capable of transporting several molecules—and other delivery vehicles as well as remote control of the permeability of their membranes is of interest in a wide range of biological applications such as transfection, while delivery and triggered release of multimolecules is relevant for a broad spectrum of therapies.[23]

METHODS

Materials. Rhodamine-dextran (7.5 kDa) and 5(6)-carboxyfluorescein (0.376 kD) were purchased from Sigma-Aldrich, Germany, and were used as received without further purification. PBS without Ca^{2+} and Mg^{2+} and with low endotoxin was purchased from Sigma-Aldrich, Germany. The Red Fluorescent Cell Linker Kit (PKH26) and other chemicals were obtained from Sigma-Aldrich, Germany.

Gold Nanoparticle Synthesis. Gold nanoparticles were synthesized using a previously reported protocol[123] by the reduction of tetrachloroaurate in the presence of sodium borohydride in toluene and stabilized by tetraoctylammonium bromide in toluene. 4-Dimethylaminopyridine was used to facilitate phase transfer of nanoparticles to water. The size of the gold nanoparticles (determined by TEM using a Zeiss Omega EM 912 at an operating voltage of 120 kV) was in the range 5−10 nm, and their zeta potential was +7.8 mV. Absorbance spectra of gold nanoparticles in water and PBS buffer were measured with a CARY 50 conc. (Varian, Germany) UV−vis spectrophotometer, Figure S1, Supporting Information. The concentration of the prepared and concentrated Au-NPs was estimated[52] to be $\sim 10^{14}$ NP/mL[3]; upon mixing with PBS buffer, nanoparticles were diluted by a factor of 10^3, thus both reducing the concentration of nanoparticles and minimizing dilution of buffer by water.

Loading RBCs with Fluorescent Dyes and Molecules. RBCs were collected from healthy volunteers and anticoagulated with ethylenediamine tetraacetate. Then the cells were washed three times with PBS, 300 mOsm, pH 8. For encapsulation in RBCs, 300 μL of RBC pellets and 300 μL of solution of Rh-dextran (10 mg/mL) and 5(6)-carboxyfluorescein (1 mg/mL) in water were mixed, resulting in hypotonic conditions (final osmotic pressure in the RBC suspension was between 140 and 160 mOsm/kg, Osmomat 030, Gonotec, Berlin, Germany). The RBCs were incubated under stirring at 4 °C for 1 h and then resealed (through reconstitution of isotonicity) by adding 30 μL of PIGPA-C solution (100 mM sodium phosphate, 5 mM adenine, 100 mM inosine, 100 mM sodium pyruvate, 100 mM glucose, and 12% sodium chloride, pH 7.4) and incubation at 37 °C for 1 h. The loaded RBCs were washed three times with PBS (300 mOsm, pH = 8, room temperature) to remove free hemoglobin and excess dyes.

Membrane Staining for Negative Control of Thermobleaching. The membrane of 5(6)-CF-loaded RBCs was stained by PKH26 using a Red Fluorescent Cell Linker Kit for general cell membrane labeling. PKH26 is a yellow-orange fluorescent dye with long aliphatic tails, which incorporates into the lipid regions of the cell membrane. The staining was performed according to the manufacturer's instructions. Briefly, RBCs and the dye solution were mixed to final concentrations of 1×10^7 cells/mL and 2×10^{-6} M PKH26, respectively. After incubation at room temperature for 5 min an equal volume of PBS with 1% BSA was added to allow binding of excess dye. Finally, the cells were washed and resuspended in PBS to a volume ratio of 50%.

Gold Nanoparticle Adsorption on RBCs. Gold nanoparticle adsorption was performed according to the following procedure. First, 1 mL of nanoparticles was further concentrated in a centrifuge at 10 kRPM for 30 min; the supernatant was collected, leaving ~50 μL of concentrated nanoparticles solution. Then, 1 μL of this concentrated nanoparticle solution was added to 300 μL of RBC solution in PBS (2.5×10^4 cells/μL). Nanoparticle adsorption took place within minutes.

Raman spectra were recorded on a WiTec confocal Raman microscope (alpha300, WiTec, Ulm, Germany) equipped with a piezo-scanner (P-500, Physik Instrumente, Karlsruhe, Germany). Incident laser power used in these measurements 10 mW; wavelength 785 nm. For Raman scattering investigation of Au-NP adsorption on RBCs the latter were used without encapsulated molecules. Multiple and repeatable readings from the same spot indicate consistency of measurements and constant binding of nanoparticles to RBCs.

Opto-nanoporation. CLSM micrographs of the RBCs were taken with a Leica confocal scanning system mounted to a Leica Aristoplan and equipped with a 100× oil immersion objective with a numerical aperture of 1.4. The excitation wavelength for 5(6)-CF was 488 nm, while that for Rh-dextran was 543 nm. For remote release of encapsulated materials a home-built setup[31] was used. The laser location was fixed, while the sample was positioned by an XYZ stage. The incident power (on the sample) of the laser operating at 830 nm was set up to 30 mW, corresponding to a power density of up to 500 kW/cm^2 (the beam radius is on the order of 1 μm; ~55% transmission[38] of the microscope objective is taken into consideration). Cells were exposed for times on the order of seconds, which is longer than the diffusion time of molecules across a characteristic size of a RBC.[74] Experiments were performed within 10 to 20 min of the nanoparticle addition.

Experiments were conducted on a large number of cells (minimum 50 cells per sample). Two types of experiments were conducted for opto-nanoporation. In the first type of experiments, RBCs were first visualized on the CLSM. Then they were transferred to the optical setup for opto-nanoporation experiments, after which RBCs were brought back to the CLSM for final visualization. These images were recorded on the CLSM and are presented in Figure 3 and Figure 5. In the second type of experiments, referred to as *in situ*, opto-nanoporation has been performed on the optical setup with a fluorescence lamp coupled for visualizing. Here, release has been conducted and observed *in situ*, *i.e.*, directly in the setup. Data recorded using this method are presented in Figure 4 and Figure S3.

Numerical simulations of temperature distribution around Au-NPs were performed on COMSOL multiphysics software using the following parameters: conductivity of water, 0.5 W/km; size of nanoparticles, 10 nm; their absorption coefficient, 0.8 (it was calculated using refractive indices for bulk gold,[124] wavelength ~520 nm); incident laser power on the objective, 30 mW; beam, ~1 μm. Thermal conductivity of surrounding medium was taken as that of water, the main constituent of cells.[37] The size (cross-section) of Au-NP aggregates was taken as 150 nm, which corresponds to the average size reached within 10 to 20 min after addition of Au-NPs. The temperature rise on the nanoparticles is directly proportional to the incident power density and absorption coefficient and inversely proportional to the distance from the nanoparticles.[34] For further calculations, we took into consideration the so-called surface-to-volume[42] or accumulative[78] heating from neighboring nanoparticles. In essence, such an approach is similar to that based on the effective medium calculation.[98] For temperature calculation the Coulomb interactions of nanoparticles, which depend on the interparticle distance and polarization of light as well as retardation effects[125] (the phase shift is small enough compared to the wavelength of light even after aggregation), were not taken into consideration. These effects are generally weaker than the surface-to-volume heating of neighboring nanoparticles.

Conflict of Interest: The authors declare no competing financial interest.

Acknowledgment. We thank P. Subedi for assistance in gold nanoparticle synthesis, R. Pitschke for TEM imaging, and A.

Kretzschmar and H. Pitas for assistance with building the setup. The support by the ZIM-KF2354402FRO (Federal Ministry for Economics and Technology of Germany) is kindly acknowledged. We also acknowledge very fruitful discussions with D. Braun (Ludwig Maximilian University, Munich, Germany) and A. Govorov (The Ohio State University, Columbus, Ohio, USA).

Supporting Information Available: Absorbance of nonaggregated Au-NPs and aggregates of Au-NPs. CLSM images of an echinocyte after release of two molecules. Frame-by-frame analysis of control of photo- and themobleaching for a sample without Au-NPs. Dynamic light scattering measurements of aggregation of Au-NPs in PBS buffer as a function of time. This material is available free of charge *via* the Internet at http://pubs.acs.org.

REFERENCES AND NOTES

1. Mann, S. Life as a Nanoscale Phenomenon. *Angew. Chem., Int. Ed.* **2008**, *47*, 5306–5320.
2. Rossi, L.; Serafini, S.; Pierige, F.; Antonelli, A.; Cerasi, A.; Fraternale, A.; Chiarantini, L.; Magnani, M. Erythrocyte-Based Drug Delivery. *Expert Opin. Drug Delivery* **2005**, *2*, 311–322.
3. Muzykantov, V. R. Drug Delivery by Red Blood Cells: Vascular Carriers Designed by Mother Nature. *Expert Opin. Drug Delivery* **2010**, *7*, 403–427.
4. Alpar, H.; Lewis, D. A. The Prolongation of the Survival Times of Mice Implanted with TLX5 Cells byTreatment with Methotrexate Encapsulated in Erythrocytes. *Biochem. Pharmacol.* **1987**, *36*, 3081–3083.
5. Staedtke, V.; Brähler, M.; Müller, A.; Georgieva, R.; Bauer, S.; Sternberg, N.; Voigt, A.; Lemke, A.; Keck, C.; Möschwitzer, J.; *et al*. *In vitro* Inhibition of Fungal Activity by Macrophage-Mediated Sequestration and Release of Encapsulated Amphotericin B Nanosupension in Red Blood Cells. *Small* **2010**, *6*, 96–103.
6. Brahler, M.; Georgieva, R.; Buske, N.; Müller, A.; Müller, S.; Pinkernelle, J.; Teichgraber, U.; Voigt, A.; Bäumler, H. Magnetite-Loaded Carrier Erythrocytes as Contrast Agents for Magnetic Resonance Imaging. *Nano Lett.* **2006**, *6*, 2505–2509.
7. Chanana, M.; Jahn, S.; Georgieva, R.; Lutz, J. F.; Bäumler, H.; Wang, D. Y. Fabrication of Colloidal Stable, Thermosensitive, and Biocompatible Magnetite Nanoparticles and Study of Their Reversible Agglomeration in Aqueous Milieu. *Chem. Matter.* **2009**, *21*, 1906–1914.
8. Grover, S. C.; Gauthier, R. C.; Skirtach, A. G. Analysis of the Behaviour of Erythrocytes in an Optical Trapping System. *Opt. Express* **2000**, *7*, 533–539.
9. Grover, S. C.; Skirtach, A. G.; Gauthier, R. C.; Grover, C. P. Automated Single-Cell Sorting System Based on Optical Trapping. *J. Biomed. Opt.* **2001**, *6*, 14–22.
10. Lindstrom, S.; Andersson-Svahn, H. Overview of Single-Cell Analyses: Microdevices and Applications. *Lab Chip* **2010**, *10*, 3363–3372.
11. Werner, M.; Merenda, F.; Piguet, J.; Salathe, R. P.; Vogel, H. Microfluidic Array Cytometer Based on Refractive Optical Tweezers for Parallel Trapping, Imaging and Sorting of Individual Cells. *Lab Chip* **2011**, *11*, 2432–2439.
12. Markov, D. E.; Boeve, H.; Gleich, B.; Borgert, J.; Antonelli, A.; Sfara, C.; Magnani, M. Human Erythrocytes as Nanoparticle Carriers for Magnetic Particle Imaging. *Phys. Med. Biol.* **2010**, *55*, 6461–6473.
13. Ahn, S.; Jung, S. Y.; Seo, E.; Lee, S. J. Gold Nanoparticle-Incorporated Human Red Blood Cells (RBCs) for X-Ray Dynamic Imaging. *Biomaterials* **2011**, *32*, 7191–7199.
14. Nikolskaya, A. V.; Nikolski, V. P.; Efimov, I. R. Gene Printer: Laser-Scanning Targeted Transfection of Cultured Cardiac Neonatal Rat Cells. *Cell Commun. Adhes.* **2006**, *13*, 217–222.
15. Blum, H. F.; Gilbert, H. W. Quantum Requirements for Photodynamic Hemolysis. *J. Cell. Comp. Physiol.* **1940**, *15*, 85–93.
16. Palumbo, G.; Caruso, M.; Crescenzi, E.; Tecce, M. F.; Roberti, G.; Colasanti, A. Targeted Gene Transfer in Eucaryotic Cells by Dye-Assisted Laser Optoporation. *J. Photochem. Photobiol. B* **1996**, *36*, 41–46.
17. Schneckenburger, H.; Hendinger, A.; Sailer, R.; Strauss, W. S.; Schmitt, M. Laser-Assisted Optoporation of Single Cells. *J. Biomed. Opt.* **2002**, *7*, 410–416.
18. Wu, T. H.; Teslaa, T.; Kalim, S.; French, C. T.; Moghadam, S.; Wall, R.; Miller, J. F.; Witte, O. N.; Teitell, M. A.; Chiou, P. Y. Photothermal Nanoblade for Large Cargo Delivery into Mammalian Cells. *Anal. Chem.* **2011**, *83*, 1321–1327.
19. Stevenson, D. J.; Gunn-Moore, F. J.; Campbell, P.; Dholakia, K. Single Cell Optical Transfection. *J. R. Soc. Interface* **2010**, *7*, 863–871.
20. Tirlapur, U. K.; Konig, K. Cell Biology—Targeted Transfection by Femtosecond Laser. *Nature* **2002**, *418*, 290–291.
21. Lukianova-Hleb, E. Y.; Oginsky, A. O.; Olson, J. S.; Lapotko, D. O. Short Laser Pulse-Induced Irreversible Photothermal Effects in Red Blood Cells. *Laser Surg. Med.* **2011**, *43*, 249–260.
22. Baffou, G.; Rigneault, H. Femtosecond-Pulsed Optical Heating of Gold Nanoparticles. *Phys. Rev. B* **2011**, *84*, 035415.
23. Delcea, M.; Mohwald, H.; Skirtach, A. G. Stimuli-Responsive LbL Capsules and Nanoshells for Drug Delivery. *Adv. Drug Delivery Rev.* **2011**, *63*, 730–747.
24. Skirtach, A. G.; Yashchenok, A. M.; Mohwald, H. Encapsulation, Release and Applications of LbL Polyelectrolyte Multilayer Capsules. *Chem. Commun.* **2011**, *47*, 12736–12746.
25. Hafner, J. H.; Nordlander, P.; Weiss, P. S. Virtual Issue on Plasmonics. *ACS Nano* **2011**, *5*, 4245–4248.
26. El-Sayed, I. H.; Huang, X. H.; El-Sayed, M. A. Selective Laser Photo-Thermal Therapy of Epithelial Carcinoma Using anti-EGFR Antibody Conjugated Gold Nanoparticles. *Cancer Lett.* **2006**, *239*, 129–135.
27. Gobin, A. M.; Lee, M. H.; Halas, N. J.; James, W. D.; Drezek, R. A.; West, J. L. Near-Infrared Resonant Nanoshells for Combined Optical Imaging and Photothermal Cancer Therapy. *Nano Lett.* **2007**, *7*, 1929–1934.
28. Urban, A. S.; Fedoruk, M.; Horton, M. R.; Radler, J.; Stefani, F. D.; Feldmann, J. Controlled Nanometric Phase Transitions of Phospholipid Membranes by Plasmonic Heating of Single Gold Nanoparticles. *Nano Lett.* **2009**, *9*, 2903–2908.
29. Bendix, P. M.; Nader, S.; Reihani, S.; Oddershede, L. B. Direct Measurements of Heating by Electromagnetically Trapped Gold Nanoparticles on Supported Lipid Bilayers. *ACS Nano* **2010**, *4*, 2256–2262.
30. Urban, A. S.; Pfeiffer, T.; Fedoruk, M.; Lutich, A. A.; Feldmann, J. Single-Step Injection of Gold Nanoparticles through Phospholipid Membranes. *ACS Nano* **2011**, *5*, 3585–3590.
31. Skirtach, A. G.; Antipov, A. A.; Shchukin, D. G.; Sukhorukov, G. B. Remote Activation of Capsules Containing Ag Nanoparticles and IR Dye by Laser Light. *Langmuir* **2004**, *20*, 6988–6992.
32. Radt, B.; Smith, T. A.; Caruso, F. Optically Addressable Nanostructured Capsules. *Adv. Mater.* **2004**, *16*, 2184–2189.
33. Angelatos, A. S.; Radt, B.; Caruso, F. Light-Responsive Polyelectrolyte/Gold Nanoparticle Microcapsules. *J. Phys. Chem. B* **2005**, *109*, 3071–3076.
34. Skirtach, A. G.; Dejugnat, C.; Braun, D.; Susha, A. S.; Rogach, A. L.; Parak, W. J.; Mohwald, H.; Sukhorukov, G. B. The Role of Metal Nanoparticles in Remote Release of Encapsulated Materials. *Nano Lett.* **2005**, *5*, 1371–1377.
35. Zasadzinski, J. A.; Wong, B.; Forbes, N.; Braun, G.; Wu, G. H. Novel Methods of Enhanced Retention in and Rapid, Targeted Release from Liposomes. *Curr. Opin. Colloid Interface Sci.* **2011**, *16*, 203–214.
36. Preiss, M. R.; Bothun, G. D. Stimuli-Responsive Liposome-Nanoparticle Assemblies. *Expert Opin. Drug Delivery* **2011**, *8*, 1025–1040.
37. Skirtach, A. G.; Munoz Javier, A.; Kreft, O.; Kohler, K.; Piera Alberola, A.; Mohwald, H.; Parak, W. J.; Sukhorukov, G. B.

Laser-Induced Release of Encapsulated Materials Inside Living Cells. *Angew. Chem., Int. Ed.* **2006**, *45*, 4612–4617.
38. Neuman, K. C.; Block, S. M. Optical Trapping. *Rev. Sci. Instrum.* **2004**, *75*, 2787–2809.
39. Hale, G. M.; Querry, M. R. Optical-Constants of Water in 200-nm to 200-mm Wavelenght Region. *Appl. Opt.* **1973**, *12*, 555–563.
40. Javier, A. M.; del Pino, P.; Bedard, M. F.; Ho, D.; Skirtach, A. G.; Sukhorukov, G. B.; Plank, C.; Parak, W. J. Photoactivated Release of Cargo from the Cavity of Polyelectrolyte Capsules to the Cytosol of Cells. *Langmuir* **2008**, *24*, 12517–12520.
41. Palankar, R.; Skirtach, A. G.; Kreft, O.; Bedard, M.; Garstka, M.; Gould, K.; Mohwald, H.; Sukhorukov, G. B.; Winterhalter, M.; Springer, S. Controlled Intracellular Release of Peptides from Microcapsules Enhances Antigen Presentation on MHC Class I Molecules. *Small* **2009**, *5*, 2168–2176.
42. Volodkin, D. V.; Madaboosi, N.; Blacklock, J.; Skirtach, A. G.; Mohwald, H. Surface-Supported Multilayers Decorated with Bio-active Material Aimed at Light-Triggered Drug Delivery. *Langmuir* **2009**, *25*, 14037–14043.
43. Skirtach, A. G.; Volodkin, D. V.; Mohwald, H. Bio-interfaces-Interaction of PLL/HA Thick Films with Nanoparticles and Microcapsules. *ChemPhysChem* **2010**, *11*, 822–829.
44. Huhn, D.; Govorov, A.; Gil, P. R.; Parak, W. J. Photostimulated Au Nanoheaters in Polymer and Biological Media: Characterization of Mechanical Destruction and Boiling. *Adv. Funct. Mater.* **2012**, *22*, 294–303.
45. Van Cutsem, E.; Peeters, M.; Verslype, C.; Filez, L.; Haustermans, K.; Janssens, J. The Medical Treatment of Colorectal Cancer: Actual Status and New Developments. *Hepatogastroenterology* **1999**, *46*, 709–716.
46. Labianca, R. F.; Beretta, G. D.; Pessi, M. A. Disease Management Considerations: Disease Management Considerations. *Drugs* **2001**, *61*, 1751–64.
47. Vergaro, V.; Scarlino, F.; Bellomo, C.; Rinaldi, R.; Vergara, D.; Maffia, M.; Baldassarre, F.; Giannelli, G.; Zhang, X. C.; Lvov, Y. M.; *et al*. Drug-Loaded Polyelectrolyte Microcapsules for Sustained Targeting of Cancer Cells. *Adv. Drug Delivery Rev.* **2011**, *63*, 847–863.
48. Magnani, M. *Erythrocyte Engineering for Drug Delivery and Targeting*; Kluwer Academic/Plenum Publishers, 2003.
49. Millan, C. G.; Bax, B. E.; Castaneda, A. Z.; Marinero, M. L. S.; Lanao, J. M. *In Vitro* Studies of Amikacin-Loaded Human Carrier Erythrocytes. *Transl. Res.* **2008**, *152*, 59–66.
50. Sternberg, N.; Georgieva, R.; Duft, K.; Bäumler, H. Surface-Modified Loaded Human Red Blood Cells for Targeting and Delivery of Drugs. *J. Microencapsul.* **2012**, *29*, 9–20.
51. Bédard, M. F.; Braun, D.; Sukhorukov, G. B.; Skirtach, A. G. Toward Self-Assembly of Nanoparticles on Polymeric Microshells: Near-IR Release and Permeability. *ACS Nano* **2008**, *2*, 1807–1816.
52. Skirtach, A. G.; Dejugnat, C.; Braun, D.; Susha, A. S.; Rogach, A. L.; Sukhorukov, G. B. Nanoparticles Distribution Control by Polymers: Aggregates *versus* Nonaggregates. *J. Phys. Chem. C* **2007**, *111*, 555–564.
53. Parakhonskiy, B. V.; Bedard, M. F.; Bukreeva, T. V.; Sukhorukov, G. B.; Mohwald, H.; Skirtach, A. G. Nanoparticles on Polyelectrolytes at Low Concentration: Controlling Concentration and Size. *J. Phys. Chem. C* **2010**, *114*, 1996–2002.
54. Khlebtsov, N. G.; Dykman, L. A.; Krasnov, Y. M.; Mel'nikov, A. G. Light Absorption by the Clusters of Colloidal Gold and Silver Particles Formed During Slow and Fast Aggregation. *Colloid J.* **2000**, *62*, 765–779.
55. Goldenberg, H.; Tranter, C. J. Heat Flow in an Infinite Medium Heated by a Sphere. *Br. J. Appl. Phys.* **1952**, *3*, 296–298.
56. Moskovits, M. Surface-Enhanced Spectroscopy. *Rev. Mod. Phys.* **1985**, *57*, 783–826.
57. Pal, S.; Depero, L. E.; Alessandri, I. Using Aggregates of Gold Nanorods in SER(R)S Experiments: an Empirical Evaluation of Some Critical Aspects. *Nanotechnology* **2010**, *21*, 425701.
58. Harz, M.; Kiehntopf, M.; Stockel, S.; Rosch, P.; Deufel, T.; Popp, J. Analysis of Single Blood Cells for CSF Diagnostics *via* a Combination of Fluorescence Staining and Micro-Raman Spectroscopy. *Analyst* **2008**, *133*, 1416–1423.
59. Mathlouthi, M.; Koenig, J. L. Vibrational-Spectra of Carbohydrates. *Adv. Carbohydr. Chem. Biochem.* **1986**, *44*, 7–89.
60. Lippert, J. L.; Gorczyca, L. E.; Meiklejohn, G. Laser Raman Spectroscopic Investigation of Phospholipid and Protein Configurations in Hemoglobin-Free Erythrocyte-Ghosts. *Biochim. Biophys. Acta* **1975**, *382*, 51–57.
61. Wood, B. R.; Caspers, P.; Puppels, G. J.; Pandiancherri, S.; McNaughton, D. Resonance Raman Spectroscopy of Red Blood Cells using Near-Infrared Laser Excitation. *Anal. Bioanal. Chem.* **2007**, *387*, 1691–1703.
62. Oleinikov, V.; Kryukov, E.; Kovner, M.; Ermishov, M.; Tuzikov, A.; Shiyan, S.; Bovin, N.; Nabiev, I. Sialylation Sensitive Bands in the Raman Spectra of Oligosaccharides and Glycoproteins. *J. Mol. Struct.* **1999**, *481*, 475–480.
63. Salomao, M.; Zhang, X.; Yang, Y.; Lee, S.; Hartwig, J. H.; Chasis, J. A.; Mohandas, N.; An, X. Protein 4.1R-Dependent Multiprotein Complex: New Insights into the Structural Organization of the Red Blood Cell Membrane. *Proc. Natl. Acad. Sci.* **2008**, *105*, 8026–8031.
64. Roseman, S. Reflections on Glycobiology. *J. Biol. Chem.* **2001**, *45*, 41527–41542.
65. Donath, E.; Gingell, D. A Sharp Cell-Surface Conformational Transition at Low Ionic-Strength Changes the Nature of the Adhesion of Enzyme-Treated Red-Blood-Cell to Hydrocarbon Interface. *J. Cell Sci.* **1983**, *63*, 113–124.
66. Bäumler, H.; Halbhuber, K. J.; Stibenz, D.; Lerche, D. Topo-Optical Investigation of Human-Erythrocyte Glycocalyx Conformational-Changed Induced by Dextran. *Biochim. Biophys. Acta* **1987**, *923*, 22–28.
67. Keller, S. L.; Pitcher, W. H.; Huestis, W. H.; McConnell, H. M. Red Blood Cell Lipids Form Immiscible Liquids. *Phys. Rev. Lett.* **1998**, *81*, 5019–5022.
68. Voet, D.; Voet, J. G. *Biochemie*; VCH: Weinheim, 1994; pp 8−9.
69. Zachowski, A. Phospholipids in Animal Eukaryotic Membranes−Transverse Asymmetry and Movement. *Biochem. J.* **1993**, *294*, 1–14.
70. Ivanov, I. T.; Brähler, M.; Georgieva, R.; Bäumler, H. Role of Membrane Proteins in Thermal Damage and Necrosis of Red Blood Cells. *Thermochim. Acta* **2007**, *456*, 7–12.
71. Elgsaeter, A.; Stokke, B. T.; Mikkelsen, A.; Branton, D. The Molecular-Basis of Erythrocyte Shape. *Science* **1986**, *234*, 1217–1223.
72. Bedard, M. F.; De Geest, B. G.; Möhwald, H.; Sukhorukov, G. B.; Skirtach, A. G. Direction Specific Release from Giant Microgel-Templated Polyelectrolyte Microcontainers. *Soft Matter* **2009**, *5*, 3927–3931.
73. Schmidt, S.; Fernandes, P. A. L.; De Geest, B. G.; Delcea, M.; Skirtach, A. G.; Mohwald, H.; Fery, A. Release Properties of Pressurized Microgel Templated Capsules. *Adv. Funct. Mater.* **2011**, *21*, 1411–1418.
74. Seksek, O.; Biwersi, J.; Verkman, A. S. Translational Diffusion of Macromolecule-Sized Solutes in Cytoplasm and Nucleus. *J. Cell Biol.* **1997**, *138*, 131–142.
75. Maity, S.; Downen, L. N.; Bochinski, J. R.; Clarke, L. I. Embedded Metal Nanoparticles as Localized Heat Sources: An Alternative Processing Approach for Complex Polymeric Materials. *Polymer* **2011**, *52*, 1674–1685.
76. Alessandri, I.; Depero, L. E. Laser-Induced Modification of Polymeric Beads Coated with Gold Nanoparticles. *Nanotechnology* **2008**, *19*, 305301.
77. Baffou, G.; Quidant, R.; de Abajo, F. J. G. Nanoscale Control of Optical Heating in Complex Plasmonic Systems. *ACS Nano* **2010**, *4*, 709–716.
78. Lee, S. E.; Lee, L. P. Nanoplasmonic Gene Regulation. *Curr. Opin. Chem. Biol.* **2010**, *14*, 623–633.
79. Yavlovich, A.; Smith, B.; Gupta, K.; Blumenthal, R.; Puri, A. Light-Sensitive Lipid-Based Nanoparticles for Drug

Delivery: Design Principles and Future Considerations for Biological Applications. *Mol. Membr. Biol.* **2010**, *27*, 364–381.
80. Coronado, E. A.; Encina, E. R.; Stefani, F. D. Optical Properties of Metallic Nanoparticles: Manipulating Light, Heat and Forces at the Nanoscale. *Nanoscale* **2011**, *3*, 4042–4059.
81. Khlebtsov, B.; Panfilova, E.; Khanadeev, V.; Bibikova, O.; Terentyuk, G.; Ivanov, A.; Rumyantseva, V.; Shilov, I.; Ryabova, A.; Loshchenov, V.; *et al*. Nanocomposites Containing Silica-Coated Gold-Silver Nanocages and Yb-2,4-Dimethoxyhematoporphyrin: Multifunctional Capability of IR-Luminescence Detection, Photosensitization, and Photothermolysis. *ACS Nano* **2011**, *5*, 7077–7089.
82. Cobley, C. M.; Chen, J. Y.; Cho, E. C.; Wang, L. V.; Xia, Y. N. Gold Nanostructures: a Class of Multifunctional Materials for Biomedical Applications. *Chem. Soc. Rev.* **2011**, *40*, 44–56.
83. Jones, M. R.; Osberg, K. D.; Macfarlane, R. J.; Langille, M. R.; Mirkin, C. A. Templated Techniques for the Synthesis and Assembly of Plasmonic Nanostructures. *Chem. Rev.* **2011**, *111*, 3736–3827.
84. Petersen, S.; Barchanski, A.; Taylor, U.; Klein, S.; Rath, D.; Barcikowski, S. Penetratin-Conjugated Gold Nanoparticles—Design of Cell-Penetrating Nanomarkers by Femtosecond Laser Ablation. *J. Phys. Chem. C* **2011**, *115*, 5152–5159.
85. Alessandri, I.; Depero, L. E. Using Plasmonic Heating of Gold Nanoparticles to Generate Local SER(R)S-active TiO_2 Spots. *Chem. Commun.* **2009**, 2359–2361.
86. Alessandri, I. Writing, Self-Healing, and Self-Erasing on Conductive Pressure-Sensitive Adhesives. *Small* **2010**, *6*, 1679–1685.
87. Fedoruk, M.; Lutich, A. A.; Feldmann, J. Subdiffraction-Limited Milling by an Optically Driven Single Gold Nanoparticle. *ACS Nano* **2011**, *5*, 7377–7382.
88. Skorb, E. V.; Skirtach, A. G.; Sviridov, D. V.; Shchukin, D. G.; Mohwald, H. Laser-Controllable Coatings for Corrosion Protection. *ACS Nano* **2009**, *3*, 1753–1760.
89. Van de Broek, B.; Grandjean, D.; Trekker, J.; Ye, J.; Verstreken, K.; Maes, G.; Borghs, G.; Nikitenko, S.; Lagae, L.; Bartic, C.; *et al*. Temperature Determination of Resonantly Excited Plasmonic Branched Gold Nanoparticles by X-ray Absorption Spectroscopy. *Small* **2011**, *7*, 2498–2506.
90. Skirtach, A. G.; Kurth, D. G.; Mohwald, H. Laser-Embossing Nanoparticles into a Polymeric Film. *Appl. Phys. Lett.* **2009**, *94*, 093106.
91. Harris, N.; Ford, M. J.; Cortie, M. B. Optimization of Plasmonic Heating by Gold Nanospheres and Nanoshells. *J. Phys. Chem. B* **2006**, *110*, 10701–10707.
92. Govorov, A. O.; Richardson, H. H. Generating Heat with Metal Nanoparticles. *Nano Today* **2007**, *2*, 30–38.
93. Kreibig, U.; Quinten, M.; Schoenauer, D. Optical-Properties of Many-Particle Systems. *Phys. Scr.* **1986**, *T13*, 84–92.
94. Quinten, M.; Kreibig, U. Optical Properties of Aggregates of Small Metal Particles. *Surf. Sci.* **1986**, *172*, 557–577.
95. Hao, E.; Schatz, G. C. Electromagnetic Fields around Silver Nanoparticles and Dimers. *J. Chem. Phys.* **2004**, *120*, 357–366.
96. Brandl, D. W.; Mirin, N. A.; Nordlander, P. Plasmon Modes of Nanosphere Trimers and Quadrumers. *J. Phys. Chem. B* **2006**, *110*, 12302–12310.
97. Chuntonov, L.; Haran, G. Trimeric Plasmonic Molecules: The Role of Symmetry. *Nano Lett.* **2011**, *11*, 2440–2445.
98. Hrelescu, C.; Stehr, J.; Ringler, M.; Sperling, R. A.; Parak, W. J.; Klar, T. A.; Feldmann, J. DNA Melting in Gold Nanostove Clusters. *J. Phys. Chem. C* **2010**, *114*, 7401–7411.
99. Lazarides, A. A.; Schatz, G. C. DNA-Linked Metal Nanosphere Materials: Structural Basis for the Optical Properties. *J. Phys. Chem. B* **2000**, *104*, 460–467.
100. Skirtach, A. G.; Karageorgiev, P.; Bedard, M. F.; Sukhorukov, G. B.; Mohwald, H. Reversibly Permeable Nanomembranes of Polymeric Microcapsules. *J. Am. Chem. Soc.* **2008**, *130*, 11572–11573.
101. Pelton, M.; Aizpurua, J.; Bryant, G. Metal-Nanoparticle Plasmonics. *Laser Photonics Rev.* **2008**, *2*, 136–159.
102. Rivera Gil, P.; del Mercato, L. L.; del-Pino, P.; Munoz-Javier, A.; Parak, W. J. Nanoparticle-Modified Polyelectrolyte Capsules. *Nano Today* **2008**, *3*, 12–21.
103. Gregersen, K. A. D.; Hill, Z. B.; Gadd, J. C.; Fujimoto, B. S.; Maly, D. J.; Chiu, D. T. Intracellular Delivery of Bioactive Molecules Using Light-Addressable Nanocapsules. *ACS Nano* **2010**, *4*, 7603–7611.
104. Pavlov, A. M.; Sapelkin, A. V.; Huang, X. Y.; P'ng, K. M. Y.; Bushby, A. J.; Sukhorukov, G. B.; Skirtach, A. G. Neuron Cells Uptake of Polymeric Microcapsules and Subsequent Intracellular Release. *Macromol. Biosci.* **2011**, *11*, 848–854.
105. Carregal-Romero, S.; Rivera-Gil, P.; Ganas, C.; Pavlov, A. M.; Sukhorukov, G. B.; Parak, W. J. NIR-Light Triggered Delivery of Macromolecules into the Cytosol. *J. Controlled Release* **2012**, 10.1016/j.jconrel.2011.12.013.
106. Lerche, D.; Baumler, H. Moderate Heat-Treatment of Only Red Blood Cells (RBC) Slows Down the Rate of RBC-RBC Aggregation in Plasma. *Biorheology* **1984**, *21*, 393–403.
107. Snabre, P.; Baumler, H.; Mills, P. Aggregation of Human Red Blood-Cells after Moderate Heat-Treatment. *Biorheology* **1985**, *22*, 185–195.
108. Coakley, W. T.; Bater, A. J.; Crum, L. A.; Deeley, J. O. T. Morphological Changes, Hemolysis and Microvesicularization of Heated Human Erythrocytes. *J. Therm. Biol.* **1979**, *4*, 85–93.
109. Gershfeld, N. L.; Murayama, M. Thermal-Instability of Red Blood-Cell Membrane Bilayers—Temperature-Dependence of Hemolysis. *J. Membr. Biol.* **1988**, *101*, 67–72.
110. Krpetic, Z.; Nativo, P.; See, V.; Prior, I. A.; Brust, M.; Volk, M. Inflicting Controlled Nonthermal Damage to Subcellular Structures by Laser-Activated Gold Nanoparticles. *Nano Lett.* **2010**, *10*, 4549–4554.
111. McIntosh, C. M.; Esposito, E. A.; Boal, A. K.; Simard, J. M.; Martin, C. T.; Rotello, V. M. Inhibition of DNA Transcription using Cationic Mixed Monolayer Protected Gold Clusters. *J. Am. Chem. Soc.* **2001**, *123*, 7626–7629.
112. Goodman, C. M.; McCusker, C. D.; Yilmaz, T.; Rotello, V. M. Toxicity of Gold Nanoparticles Functionalized with Cationic and Anionic Side Chains. *Bioconjugate Chem.* **2004**, *15*, 897–900.
113. Gorelikov, I.; Field, L. M.; Kumacheva, E. Hybrid Microgels Photoresponsive in the Near-Infrared Spectral Range. *J. Am. Chem. Soc.* **2004**, *126*, 15938–15939.
114. Perez-Juste, J.; Pastoriza-Santos, I.; Liz-Marzan, L. M.; Mulvaney, P. Gold Nanorods: Synthesis, Characterization and Applications. *Coord. Chem. Rev.* **2005**, *249*, 1870–1901.
115. Skirtach, A. G.; Karageorgiev, P.; De Geest, B. G.; Pazos-Perez, N.; Braun, D.; Sukhorukov, G. B. Nanorods as Wavelength-Selective Absorption Centers in the Visible and Near-Infrared Regions of the Electromagnetic Spectrum. *Adv. Mater.* **2008**, *20*, 506–510.
116. Leung, S. J.; Kachur, X. M.; Bobnick, M. C.; Romanowski, M. Wavelength-Selective Light-Induced Release from Plasmon Resonant Liposomes. *Adv. Funct. Mater.* **2011**, *21*, 1113–1121.
117. Yashchenok, A. M.; Bratashov, D. N.; Gorin, D. A.; Lomova, M. V.; Pavlov, A. M.; Sapelkin, A. V.; Shim, B. S.; Khomutov, G. B.; Kotov, N. A.; Sukhorukov, G. B.; *et al*. Carbon Nanotubes on Polymeric Microcapsules: Free-Standing Structures and Point-Wise Laser Openings. *Adv. Funct. Mater.* **2010**, *20*, 3136–3142.
118. Peters, R.; Louzao, I.; van Hest, J. C. M. From Polymeric Nanoreactors to Artificial Organelles. *Chem. Sci.* **2012**, *3*, 335–342.
119. Amstad, E.; Reimhult, E. Nanoparticle Actuated Hollow Drug Delivery Vehicles. *Nanomedicine* **2012**, *7*, 145–164.
120. Chen, Y. J.; Bose, A.; Bothun, G. D. Controlled Release from Bilayer-Decorated Magnetoliposomes *via* Electromagnetic Heating. *ACS Nano* **2010**, *4*, 3215–3221.

121. Amstad, E.; Kohlbrecher, J.; Muller, E.; Schweizer, T.; Textor, M.; Reimhult, E. Triggered Release from Liposomes through Magnetic Actuation of Iron Oxide Nanoparticle Containing Membranes. *Nano Lett.* **2011**, *11*, 1664–1670.
122. Katagiri, K.; Imai, Y.; Koumoto, K.; Kaiden, T.; Kono, K.; Aoshima, S. Magnetoresponsive On-Demand Release of Hybrid Liposomes Formed from Fe_3O_4 Nanoparticles and Thermosensitive Block Copolymers. *Small* **2011**, *7*, 1683–1689.
123. Gittins, D. I.; Caruso, F. Spontaneous Phase Transfer of Nanoparticulate Metals from Organic to Aqueous Media. *Angew. Chem., Int. Ed.* **2001**, *40*, 3001–3004.
124. Johnson, P. B.; Christy, R. W. Optical Constants of Noble Metals. *Phys. Rev. B* **1972**, *6*, 4370–4379.
125. Ghosh, S. K.; Pal, T. Interparticle Coupling Effect on the Surface Plasmon Resonance of Gold Nanoparticles: From Theory to Applications. *Chem. Rev.* **2007**, *107*, 4797–4862.